Vohra, Anurag; Khanam, Afrina; Slotte, Jonatan; Makkonen, Ilja; Pourtois, Geoffrey; Loo, Roger; Vandervorst, Wilfried

Evolution of phosphorus-vacancy clusters in epitaxial germanium

Published in:
Journal of Applied Physics

DOI:
10.1063/1.5054996

Published: 14/01/2019

Document Version
Publisher's PDF, also known as Version of record

Please cite the original version:
Vohra, A., Khanam, A., Slotte, J., Makkonen, I., Pourtois, G., Loo, R., & Vandervorst, W. (2019). Evolution of phosphorus-vacancy clusters in epitaxial germanium. *Journal of Applied Physics*, *125*(2), [025701]. https://doi.org/10.1063/1.5054996

Journal of Applied Physics

Evolution of phosphorus-vacancy clusters in epitaxial germanium

Cite as: J. Appl. Phys. **125**, 025701 (2019); https://doi.org/10.1063/1.5054996
Submitted: 05 September 2018 . Accepted: 13 December 2018 . Published Online: 08 January 2019

Anurag Vohra, Afrina Khanam, Jonatan Slotte, Ilja Makkonen, Geoffrey Pourtois, Roger Loo, and Wilfried Vandervorst

Journal of Applied Physics ARTICLE scitation.org/journal/jap

Evolution of phosphorus-vacancy clusters in epitaxial germanium

Cite as: J. Appl. Phys. **125**, 025701 (2019); doi: 10.1063/1.5054996
Submitted: 5 September 2018 · Accepted: 13 December 2018 ·
Published Online: 8 January 2019

Anurag Vohra,[1,2,a)] Afrina Khanam,[3] Jonatan Slotte,[3] Ilja Makkonen,[3] Geoffrey Pourtois,[2,4] Roger Loo,[2] and Wilfried Vandervorst[1,2]

AFFILIATIONS

[1]Institute for Nuclear and Radiation Physics, K.U. Leuven, Celestijnenlaan 200D, B-3001 Leuven, Belgium
[2]Imec vzw, Kapeldreef 75, B-3001 Leuven, Belgium
[3]Department of Applied Physics, Aalto University, P.O. Box 15100, FI-00076 Aalto, Finland
[4]Department of Chemistry, Plasmant Research Group, University of Antwerp, B-2610 Wilrijk-Antwerp, Belgium

[a)]**Electronic mail:** anurag.vohra@kuleuven.be

ABSTRACT

The E centers (dopant-vacancy pairs) play a significant role in dopant deactivation in semiconductors. In order to gain insight into dopant-defect interactions during epitaxial growth of *in situ* phosphorus doped Ge, positron annihilation spectroscopy, which is sensitive to open-volume defects, was performed on Ge layers grown by chemical vapor deposition with different concentrations of phosphorus ($\sim 1\times10^{18}$–$1\times10^{20}\,cm^{-3}$). Experimental results supported by first-principles calculations based on the two component density-functional theory gave evidence for the existence of mono-vacancies decorated by several phosphorus atoms as the dominant defect type in the epitaxial Ge. The concentration of vacancies increases with the amount of P-doping. The number of P atoms around the vacancy also increases, depending on the P concentration. The evolution of P_n–V clusters in Ge contributes significantly to the dopant deactivation.

I. INTRODUCTION

Silicon has been the forte of the semiconductor industry due to its pivotal role in electronics. However, the downscaling of metal-oxide-semiconductor (MOS) devices and the demand for new materials and device concepts have renewed the interest in Ge and other group IV alloys as potential candidates for both logic and photonic device applications.[1–3] One such interest is the introduction of highly phosphorus (P)-doped Ge as the source-drain (S/D) material for n-Ge FinFETs or Gate-All-Around (GAA) devices. P-doping is favored in Ge due to its higher solid solubility as compared to other group V elements. On the other hand, the solubility limit of P in Ge is only limited to $7\times10^{19}\,cm^{-3}$ at 800 °C.[4] However, required active doping levels in current n-Ge S/D schemes are above $1\times10^{20}\,cm^{-3}$. One of the strategies to boost the active dopant concentration is to move the growth process away from thermal equilibrium. Low temperature (< 400 °C) epitaxial growth of Ge:P films[5] using high-order precursors, e.g., Ge_2H_6 enables the incorporation of phosphorous concentrations above $1\times10^{20}\,cm^{-3}$. However, the low dopant activation in such as-grown layers is still the major bottleneck and the subject of the present investigation. Alternative process schemes, e.g., Ge:P δ-doping[6] or using *post–epi* implantation, rapid thermal annealing/laser (or flash lamp) annealing,[7–9] result in enhanced P activation ~ 2–$3\times10^{20}\,cm^{-3}$. These process schemes do show improved activation; however, they are difficult to implement in the final device flow. There is a high risk of surface reflow and dopant diffusion in Ge channels[10] due to the high thermal budgets, e.g., in the case of patterned fin structures in n-Ge FinFET technology. In addition, the fabrication schemes make use of process steps, which result in either non-conformal doping or non-selective growth toward oxide and nitride surfaces.

A lot of theoretical advancements have been made to understand the dopant-defect interaction in Ge.[11–13] Dopant deactivation in Ge is often referred to in the literature to arise from the formation of dopant-vacancy (V) clusters.[14,15]

However, only a few studies correlate both experiments and simulations to explain the type of defects and give the fingerprint of their constituents. Kujala *et al.*[16] studied vacancy-donor complexes in heavily n-type Ge samples, following long, high temperature diffusion anneals of P, As, and Sb profiles. This method is limited by the solid solubility at the diffusion temperature and the diffusion is in principle happening at thermal equilibrium. Hence, this is not a method that can be used to produce very high charge carrier concentrations. The alternative strategy is to move the growth process to the non-equilibrium regime, which is the method discussed in this study. The chosen growth method (Chemical Vapor Deposition) does allow conformal doping and selective growth toward oxide and nitride surfaces. On the other hand, Kalliovaara *et al.*[17] studied donor deactivation in As-implanted and laser-annealed Ge by the formation of As-divacancy clusters. The lack of electrical activation observed in our *in situ* P-doped Ge layers[5] motivated the present work to investigate the presence of any P-related defect (such as P-vacancy cluster) as the main cause of these observations.

In this paper, we apply positron annihilation spectroscopy (PAS) to study open-volume defects (i.e., vacancies) in epitaxial P-doped Ge layers. Positrons, when implanted in condensed matter, get trapped at vacancies due to the repulsion from ion cores of the host lattice. They annihilate with electrons and emit two 511 keV γ quanta.[18] The annihilating γ quanta give information about the momentum (p) distribution of the electrons, which can be analyzed to identify the size and chemical environment of the defect.[18] The momentum distribution of electron-positron pairs annihilating at open-volume defects differs from that of electron-positron pairs in the defect-free bulk material.[18] Our results show an increased concentration of mono-vacancy defects in Ge epitaxial layers with increasing P-doping. We also show that the number of P atoms as the first nearest neighbors to the vacancy also increases with P-doping. Based on these observations, we conclude that the occurrence of P_n–V clusters contributes significantly to the dopant deactivation in Ge.

II. GROWTH METHOD AND MATERIAL CHARACTERIZATION DETAILS

We studied Ge:P layers grown at 440 °C on 0.6 μm thick Ge-buffered Si (001) substrates using a 300 mm industrial standard RPCVD tool with GeH_4 and PH_3 as gas precursors (ASM Intrepid XP™). The growth conditions were kept identical at the exception of the partial pressure of PH_3, which was tuned to reach different concentration levels. The associated material properties of the studied layers: namely, the active carrier concentration (from μHall measurements), the total P content, and thickness of the films from Secondary Ion Mass Spectrometry (SIMS) are summarized in Table I.

Monoenergetic positrons (0.5–25 keV) obtained from a low-energy positron beam were used to measure all samples with Doppler Broadening Spectroscopy (DOBS), from here on referred to as "normal-Doppler." The shape of the annihilation spectrum was described using the conventional S and W parameters.[18] The S and W parameters reflect changes in low momentum (valence electrons, S) and high momentum (core electrons, W) distribution of the annihilating electron-positron pairs. The integration windows for the S and W parameters were set to ($0 < p < 0.5$ a.u.) and ($1.5 < p < 4.0$ a.u.), where a.u. stands for atomic units. All samples were measured with 2D Coincidence Doppler Broadening Spectroscopy (CDOBS),[19] from here on referred to as "coincidence-Doppler"; using a positron implantation energy of 4.5 keV. We normalized the reported data for both normal and coincidence-Doppler measurements with respect to a positron (e^+)-trap-free germanium which was used as the reference (from here on referred to as "Ge-reference"). For a more elaborative specification on PAS measurements, the reader is referred to Refs. 20–22.

TABLE I. Layer properties: thickness (t), Hall carrier concentration, and total P concentration of Ge:P films. The table also lists estimated vacancy concentrations and effective positron diffusion lengths (L_{eff}) acquired from normal-Doppler measurements.

Sample	t (nm)	Hall concentration (cm^{-3})	P total (cm^{-3})	Vacancy concentration (cm^{-3})	L_{eff} (nm)
A	100	2.6×10^{18}	2.9×10^{18}	1.6×10^{18}	60
B	112	3.4×10^{19}	6.2×10^{19}	1.7×10^{19}	20
C	112	2.7×10^{19}	1.1×10^{20}	2.5×10^{19}	16

III. COMPUTATIONAL DETAILS

We complement our experimental PAS studies on Ge:P films with first-principles simulations. Electronic structure calculations were carried out using the Vienna *ab initio* Simulation Package (VASP) employing the projector augmented wave (PAW) method.[23–26] The systems were modeled using a cubic supercell made of 216 Ge atoms. A 300 eV plane-wave kinetic energy cut off and a sampling of the Brillouin zone (BZ) at the Γ point were used in combination with the Heyd–Scuseria–Ernzerhof (HSE06)[27] hybrid functional. The fraction of non-local Hartree-Fock potential and screening parameter, μ, were set to their default values of 25% and 0.207 $Å^{-1}$ respectively. To calculate the annihilation characteristics of P_n–V clusters in Ge, we have used the so-called "conventional-scheme"[22] (CS) within zero-positron-density ($n_+ \to 0$) limit of the two-component density-functional theory[28] (TCDFT). We assume that the positron does not affect the average electron density. In positron modeling, we use the LDA approximations by Boronski and Nieminen *et al.*[28] Momentum densities were evaluated using the model by Alatalo *et al.*[29] The defect systems were relaxed taking into account the repulsive forces of positron on ions. Before comparing with the experiment, computational spectra are convoluted with the experimentally determined detector resolution of the coincidence-Doppler system. For a comprehensive description of our computational scheme, the reader is referred to Refs. 30 and 31 and the references therein.

IV. RESULTS AND DISCUSSION

A. PAS analysis on Ge:P layers

Figure 1 shows the normalized W parameters as a function of positron implantation energy E for different P-doped Ge samples. Approximately 1×10^6 annihilation counts were obtained for each incident positron energy. Calculated Makhov profile[32] for positrons as a function of depth in Ge at 4.5 and 10 keV incident positron energy are shown in Fig. 2. Implantation distribution of slow monoenergetic positrons was calculated using Eqs. (2) and (3) in Ref. 33. Based on the width of these profiles, one can assume that the W parameters for $E \leq 4.5$ keV correspond to the annihilation of positrons at the surface and in the layer of interest (i.e., P-doped Ge). For $5 \leq E \leq 10$ keV, the measured W parameters correspond to a superposition of positron annihilation at the surface, in the epitaxial Ge:P layer and the underlying Ge-virtual substrate (VS). The decreasing W values above 10 keV are due to the annihilation of positrons in the silicon substrate. In this paper, we will restrict our discussion to the type and chemical environment of the defects in the Ge:P epitaxial layers.

The W-values (normalized to the case of defect-free Ge-reference) are shown in Fig. 1. Clearly, a dependence on the P-doping concentration can be seen. Nevertheless, in all cases, a steep decay is present corresponding to the region from the surface to the entire Ge:P layer. This indicates that the effective diffusion lengths L_{eff} of the positrons are smaller than the layer thicknesses (100–112 nm) and therefore also smaller than the value of the diffusion length ($L_B = 185$ nm) in defect-free bulk Ge.[34,35] The steeper the slope, the shorter the diffusion lengths.[18] The measured W(E) data in Fig. 1 were analyzed by the VEPFIT program developed by

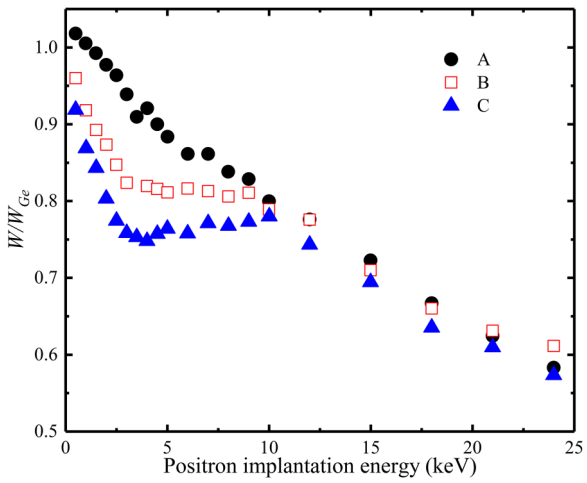

FIG. 1. *W* parameter vs positron implantation energy for epitaxial Ge samples with different P concentrations (Table I), scaled to the Ge-reference. Calculated distribution of implanted monoenergetic positrons as the function of depth is shown in Fig. 2.

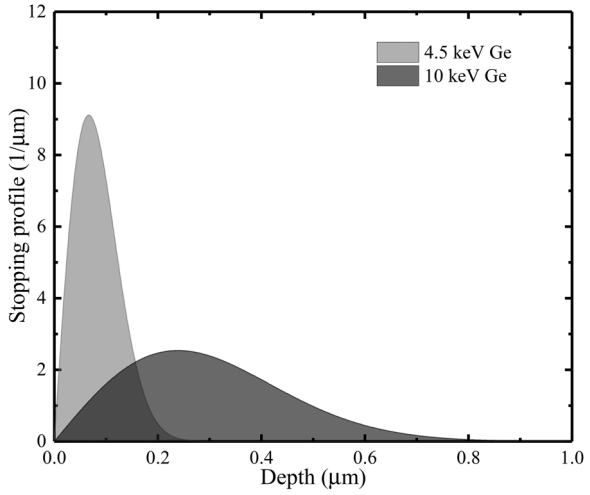

FIG. 2. Distribution of implanted positrons as the function of depth in Ge at 4.5 and 10 keV incident positron energy.

van Veen *et al.*[36] in order to estimate the effective diffusion lengths of positrons in Ge:P layers. The latter was used to evaluate the concentration of vacancies as done in Ref. 37. The estimated values of L_{eff} and the vacancy concentrations are listed in Table I. The obtained values can only be considered as estimates, since the fitting procedure to the experimental data gives only an average value for the effective diffusion length in the layer. Indeed, the resulting diffusion lengths (16–60 nm) are smaller as compared to the defect-free Ge-reference. Since positron annihilation is mainly dominated by defects, the minima in the W parameters for samples B and C at $E = 4.5$ keV shows that in the Ge:P layers, the local electron density is reduced due to missing atoms in the lattice (i.e., all positrons implanted in the Ge:P epitaxial layers annihilate at vacancy-defects and no delocalized state is observed). The estimated vacancy concentrations are in the 10^{18}–10^{19} cm^{-3} range, scale with the P-doping level and sufficiently high to deactivate a major part of the P-doping, keeping in mind that up to four P atoms can bond to one vacancy.

In order to identify the defect type and its constituent atoms, we measured all samples with coincidence-Doppler at an incident positron energy of 4.5 keV. With this energy, the positron annihilation is dominated by annihilation within the Ge:P epitaxial layers. Figure 3 shows the measured ratio plots for Ge:P layers with different P concentrations. To obtain the ratio plots, the measured coincidence-Doppler spectra were normalized with respect to the spectrum of the positron-trap-free Ge-reference. The intensities at low ($0 < p < 0.5$ a.u.) and high ($p > 1.5$ a.u.) momenta of the ratio spectra correspond mainly to the positrons annihilating with valence and core electrons, respectively.[18] The intensities measured in low momenta (S-region) are too low for anything bigger than a mono-vacancy defect. This conclusion is based on the fact that intensities in the low momentum region are

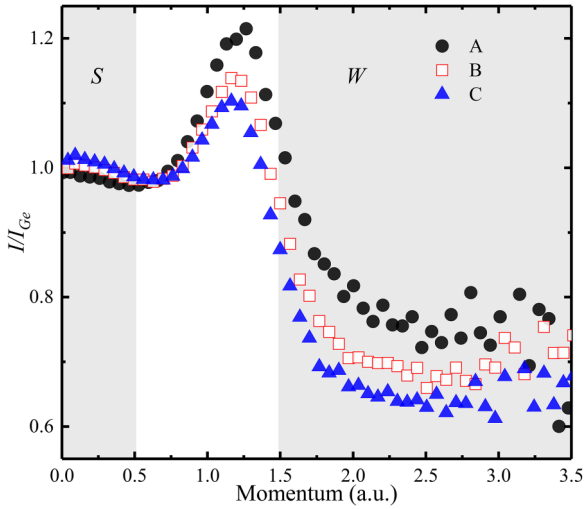

FIG. 3. Experimental ratio plots for Ge:P epitaxial layers with different P concentrations (scaled to a defect-free Ge-bulk reference) measured at an incident positron energy of 4.5 keV. The integration windows for the valence annihilation parameter (*S*) and the core annihilation parameter (*W*) are indicated by the shaded regions.

comparatively higher for larger open-volume defects than a mono-vacancy as shown in Ref. 17 for V_2-As_n complexes in Ge.

For each missing atom in the lattice (i.e., vacancies), the core electrons are obviously absent. This results in a locally reduced electron density, which in turn leads to a decreased probability of positron annihilation with core electrons. The electron configuration of Ge is $[Ar]3d^{10}4s^24p^2$, the 3*d* electron shell is the main contributor to the electron-momentum distribution at high momenta. Indeed, we observed a decreased intensity at high momenta in all Ge:P samples due to the missing contribution from the 3*d* shell electrons of Ge (Fig. 3). In addition, we do see a trend, i.e., decreasing intensity at high momenta with increasing P-doping, which implies that the chemical environment around mono-vacancy defects changes with P-doping.

B. Comparison of experimental and computational results

To interpret the coincidence-Doppler spectra in Fig. 3, we modeled the interaction of open-volume defects, primarily the mono-vacancy, with alien phosphorus atoms in a 216 atoms Ge cell. Experimentally, it has been demonstrated that mono-vacancies are unstable in Ge already above 200 K.[38] However, the situation is altered when both mono-vacancies and phosphorus atoms are present in the system with the latter having a strong affinity toward the former. In this case, the energy of the different configurations (P at various radial distances around a vacancy) is the lowest when the P atom is placed as a first nearest neighbor with respect to the position of the vacancy. The dopant-defect attraction was determined by calculating their binding energies (E_b) using Eq. (1) in Ref. 11. A negative binding energy indicates that the defect cluster is stable. Table II lists the calculated binding energies of various phosphorus-vacancy clusters in Ge for the neutral and the doubly negatively charged vacancy calculated using HSE06 and GGA (only neutral vacancy). It is evident that the cluster becomes more stable as the number of P atoms around the vacancy increases, with the most stable configuration being the one where a vacancy is enveloped by four P atoms. It must be noted that binding energies of P_n–V clusters are often underestimated in the literature[39] for generalized gradient approximation (GGA) using exchange-correlation functional proposed by Perdew–Burke–Ernzerhof,[40] which treats Ge as a metallic system in DFT. We tuned the amount of non-local Hartree-Fock exchange interaction (25%) for hybrid functional HSE06 to match the experimental value of the indirect band gap (0.74 eV) at 0 K. Clearly, P_n–V clusters are a factor ~ 2.5 stronger (Table II) than estimated using GGA.

Subsequently, we proceed by calculating the positron annihilation characteristics for phosphorus atoms around the vacancy and this for all minimum energy configurations is listed in Table II. Figure 4 shows the calculated ratio curves for the neutral and doubly negatively charged mono-vacancy and various P_n–V clusters in Ge. For comparison, we also calculated the ratio plots for a divacancy (V_2) decorated by one P atom. Let us first discuss the case of V^0 and V^{-2} (black solid line and black dashed line in Fig. 4). A missing atom in the Ge lattice leads to a reduced intensity at high momenta due to the missing contribution from the absent core electrons of Ge. For charged defects, the inward relaxation of atoms around the vacancy is promoted further as compared to the neutral defect. This leads to a smaller open-volume of the defect and an enhanced shoulder in the ratio curve at a momentum of ~ 1.2 a.u. (black dashed line). For P_n–V clusters, the intensity at high momenta decreases drastically with an increase in the number of P atoms around the vacancy (red curves). The electronic configuration of phosphorus consists only of *s* and *p* orbitals. Hence, for each P atom around the vacancy, the annihilation probability of positrons with high momentum 3*d* electrons of Ge decreases. On the other hand, for even larger open-volume defects like V_2 (black dotted curve) and P–V_2 (blue transparent curve), the annihilation intensities are considerably higher (lower) at low (high) momenta as

TABLE II. Binding energies (E_b) of phosphorus-vacancy clusters in Ge for the neutral [V^0] and doubly negatively charge vacancy [V^{-2}] calculated using GGA (only [V^0]) and HSE06. In parenthesis (E_b) values of Sb-vacancy clusters.

Cluster	E_b (eV) GGA [V^0]	E_b (eV) HSE06 [V^0]	E_b (eV) HSE06 [V^{-2}]
PV (SbV^a)	−0.42	−1.12 (− 1.27)	−0.79
P_2V (Sb_2V)	−0.86	−2.38 (− 2.58)	−1.65
P_3V (Sb_3V)	−1.33	−3.32 (− 3.78)	...
P_4V (Sb_4V)	−1.93	−4.64 (− 5.04)	...

[a]Codoping with Sb to boost P activation in Ge.

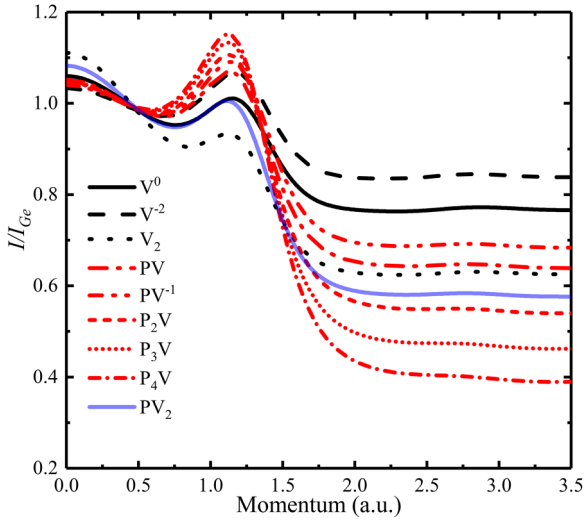

FIG. 4. Calculated ratio curves for the neutral [V^0] and doubly negatively [V^{-2}] charged mono-vacancy, divacancy (V_2), and various phosphorous-(di)vacancy complexes in Ge. Defect-free Ge-bulk was used as the reference for normalization and the spectra were convoluted with experimentally determined detector resolution of the coincidence-Doppler system.

compared to corresponding mono-vacancy clusters, V^0 (black solid line), and P–V (red dash dot curve), respectively. It is noted that similar calculations have been reported using GGA functional in Ref. 16. We draw a conclusion that trends in the momentum distribution of P_n–V clusters are not affected by the choice of exchange-correlation functional (GGA or HSE06).

The reasonable agreement between calculated ratio curves for various phosphorus-vacancy complexes in Ge with our experimental results provides evidence for the existence of P_n–V clusters in Ge:P epitaxial layers. This can be primarily concluded from their reduced contribution toward electron-momentum distribution in measured ratio curves as shown in Fig. 3. The continuous decrease in intensity with increasing P concentration as seen at high momenta substantiates the evidence that the number of P atoms around the vacancy increases with P concentration. There are at least 2 P atoms around the mono-vacancy for highly doped samples (B and C in Table I). On the other hand, the estimated concentration of vacancies, when multiplied by the number of P atoms around them (e.g., 2 and 3 P atoms for samples B and C, respectively) approximately give the same concentration of deactivated dopant's as obtained experimentally from the difference between the total P-doping level from SIMS and the active carrier concentration from μHall measurements. Nonetheless, it must be kept in mind that simulated spectra in Fig. 4 are only used for understanding trends in the experimental data (Fig. 3). In the simulations, only one type of defect is modeled under periodic boundary conditions, whereas in experimental spectra, there is a distribution of defects in the Ge:P layers. For example, sample C with the highest P-doping seems to contain a dominant defect with three P atoms around the vacancy. However, P_2–V or P_1–V clusters could also exist. The experimental spectrum shown in Fig. 3 is a superposition of positrons annihilating in P_n–V clusters within the Ge epilayer. In addition, positrons annihilating at the surface and in the Ge-VS can also influence the intensity in the momentum distribution.

V. CONCLUSIONS

In conclusion, our positron annihilation experiments together with theoretical calculations confirm the presence of high concentrations of vacancies which are incorporated with the P-doping in Ge:P epitaxial layers grown by means of CVD. The concentration of open-volume defects scales with an increasing P-doping level, which in turn suggests that the P atom is incorporated together with a vacancy. The mono-vacancy sized defects are passivated by 1-3 P atoms depending on the P-doping level. This, in turn, increases the concentration of P_n–V clusters compared to the active carrier concentration at high doping levels causing severe dopant deactivation in Ge. Point defect engineering strategies, e.g., codoping with Sb (or As), might help in improving the P activation in Ge. In essence, Sb has more attraction for vacancies than P atoms (stronger E_b values for Sb_n–V complexes than corresponding P_n–V clusters, see Table II). We speculate that Sb could passivate a large concentration of vacancies in a codoped system and might help in boosting the free carrier concentration.

SUPPLEMENTARY MATERIAL

A short overview of main equations used in this manuscript is provided in the supplementary material.

ACKNOWLEDGMENTS

The imec IIAP core CMOS program members, imec pilot line, and local authorities are acknowledged for their support. I.M. acknowledges financial support from the Academy of Finland (Project Nos. 285809, 293932, and 319178). CSC–IT Center for Science, Finland, is acknowledged for providing the computational resources. A.V. acknowledges long stay abroad grant from the Research Foundation—Flanders (Application No. V410518N).

REFERENCES

[1]D. P. Brunco, B. DeJaeger, G. Eneman, J. Mitard, G. Hellings, A. Satta, V. Terzieva, L. Souriau, F. E. Leys, G. Pourtois, M. Houssa, G. Winderickx, E. Vrancken, S. Sioncke, K. Opsomer, G. Nicholas, M. Caymax, A. Stesmans, J. v. Steenbergen, P. Mertens, M. Meuris, and M. M. Heyns, J. Electrochem. Soc. **155**(7), H552 (2008).
[2]G. He and H. A. Atwater, Phys. Rev. Lett. **79**, 1937 (1997).
[3]R. Loo, B. Vincent, F. Gencarelli, C. Merckling, A. Kumar, G. Eneman, L. Witters, W. Vandervorst, M. Caymax, M. M. Heyns, and A. Thean, ECS J. Solid State Sci. Technol. **2**(1), N35 (2013).
[4]R. W. Olesinski, N. Kanani, and G. J. Abbaschian, Bull. Alloy Phase Diagrams **6**, 262 (1985).
[5]Y. Shimura, S. A. Srinivasan, D. v. Thourhout, R. v. Deun, M. Pantouvaki, J. V. Campenhout, and R. Loo, Thin Solid Films **602**, 56 (2016).

[6]G. Mattoni, W. M. Klesse, G. Capellini, M. Y. Simmons, and G. Scappucci, ACS Nano **7**, 11310 (2013).
[7]S. H. Huang, F. L. Lu, W. L. Huang, C. H. Huang, and C. W. Liu, IEEE Electron Device Lett. **36**, 1114 (2015).
[8]R. Milazzo, G. Impellizzeri, D. Piccinotti, D. De Salvador, A. Portavoce, A. La Magna, G. Fortunato, D. Mangelinck, V. Privitera, A. Carnera, and E. Napolitani, Appl. Phys. Lett. **110**, 011905 (2017).
[9]S. Prucnal, F. Liu, M. Voelskow, L. Vines, L. Rebohle, D. Lang, Y. Berencén, S. Andric, R. Boettger, M. Helm, S. Zhou, and W. Skorupa, Sci. Rep. **6**, 27643 (2016).
[10]S. Brotzmann and H. Bracht, J. Appl. Phys. **103**, 033508 (2008).
[11]A. Chroneos, R. W. Grimes, B. P. Uberuaga, S. Brotzmann, and H. Bracht, Appl. Phys. Lett. **91**, 192106 (2007).
[12]A. Chroneos, H. Bracht, R. W. Grimes, and B. P. Uberuaga, Appl. Phys. Lett. **92**, 172103 (2008).
[13]C. Janke, R. Jones, S. Öberg, and P. R. Briddon, Phys. Rev. B **77**, 195210 (2008).
[14]H. A. Tahini, A. Chroneos, R. W. Grimes, U. Schwingenschlogl, and H. Bracht, J. Phys. Chem. Chem. Phys. **15**, 367 (2013).
[15]J. Vanhellemont, P. Śpiewak, and K. Sueoka, J. Appl. Phys. **101**, 036103 (2007).
[16]J. Kujala, T. Südkamp, J. Slotte, I. Makkonen, F. Tuomisto, and H. Bracht, J. Phys. Condens. Matter **28**, 335801 (2016), see http://stacks.iop.org/0953-8984/28/i=33/a=335801.
[17]T. Kalliovaara, J. Slotte, I. Makkonen, J. Kujala, F. Tuomisto, R. Milazzo, G. Impellizzeri, G. Fortunato, and E. Napolitani, Appl. Phys. Lett. **109**, 182107 (2016).
[18]R. Krause-Rehberg and H. S. Leipner, *Positron Annihilation in Semiconductors* (Springer-Verlag, Berlin, 1999).
[19]J. R. MacDonald, K. Lynn, R. Boie, and M. Robbins, Nucl. Instrum. Methods **153**, 189 (1978).
[20]F. Tuomisto and I. Makkonen, Rev. Mod. Phys. **85**, 1583 (2013).
[21]P. J. Schultz and K. G. Lynn, Rev. Mod. Phys. **60**, 701 (1988).
[22]M. J. Puska and R. M. Nieminen, Rev. Mod. Phys. **66**, 841 (1994).
[23]P. E. Blöchl, Phys. Rev. B **50**, 17953 (1994).
[24]G. Kresse and J. Furthmüller, Phys. Rev. B **54**, 11169 (1996).
[25]G. Kresse and J. Furthmüller, Comput. Mater. Sci. **6**, 15 (1996).
[26]G. Kresse and D. Joubert, Phys. Rev. B **59**, 1758 (1999).
[27]J. Heyd, G. E. Scuseria, and M. Ernzerhof, J. Chem. Phys. **118**, 8207 (2003).
[28]E. Boroński and R. M. Nieminen, Phys. Rev. B **34**, 3820 (1986).
[29]M. Alatalo, B. Barbiellini, M. Hakala, H. Kauppinen, T. Korhonen, M. J. Puska, K. Saarinen, P. Hautojärvi, and R. M. Nieminen, Phys. Rev. B **54**, 2397 (1996).
[30]I. Makkonen, M. Hakala, and M. J. Puska, J. Phys. Chem. Solids **66**, 1128 (2005).
[31]I. Makkonen, M. Hakala, and M. J. Puska, Phys. Rev. B **73**, 035103 (2006).
[32]S. Valkealahti and R. M. Nieminen, Appl. Phys. A **32**, 95 (1983).
[33]G. C. Aers, J. Appl. Phys. **76**, 1622 (1994).
[34]C. Corbel, M. Stucky, and P. Moser, Ann. Chim. **10**(8), 733 (1985).
[35]E. Soininen, J. Mäkinen, D. Beyer, and P. Hautojärvi, Phys. Rev. B **46**, 13104 (1992).
[36]A. van Veen, H. Schut, J. d. Vries, R. A. Hakvoort, and M. R. Ijpma, AIP Conf. Proc. **218**, 171 (1991).
[37]S. Eichler, J. Gebauer, F. Börner, A. Polity, R. Krause-Rehberg, E. Wendler, B. Weber, W. Wesch, and H. Börner, Phys. Rev. B **56**, 1393 (1997).
[38]J. Slotte, S. Kilpeläinen, F. Tuomisto, J. Räisänen, and A. N. Larsen, Phys. Rev. B **83**, 235212 (2011).
[39]A. Chroneos, R. W. Grimes, H. Bracht, and B. P. Uberuaga, J. Appl. Phys. **104**, 113724 (2008).
[40]J. P. Perdew, K. Burke, and M. Ernzerhof, Phys. Rev. Lett. **77**, 3865 (1996).